Supporting Information for "Fluorescence thermometry enhanced by the quantum coherence of single spins in diamond"

David M. Toyli,[1] Charles F. de las Casas,[1,*] David J. Christle,[1,*]
Viatcheslav V. Dobrovitski,[2] and David D. Awschalom[1,3,†]

[1]*Center for Spintronics and Quantum Computation, University of California, Santa Barbara, CA 93106, United States*

[2]*Ames Laboratory, US Department of Energy, Ames, Iowa 50011, United States*

[3]*Institute for Molecular Engineering, University of Chicago, Chicago, Illinois 60637, United States*

Contents

I. EXPERIMENTAL TECHNIQUES

The NV centers were addressed in a confocal microscope with a 0.7 NA microscope objective that allowed sufficient clearance for a resistive temperature detector (RTD) to be adhered to the diamond surface. The NV centers were optically excited with a 532 nm continuous-wave laser. For pulsed spin resonance measurements the timing of the experiment was controlled by an arbitrary waveform generator. The laser was modulated using an acousto-optic modulator; the electrical signal from the AOM driver was optimized with a diode-based filter to provide high optical extinction in a single pass. For the zero field experiments microwaves were supplied by a single signal generator gated with a mixer and switch in series. For the finite field experiments two signal sources, each independently gated with a mixer and a switch, were combined using a power splitter. In all experiments the microwave signals were amplified and delivered to a Ti/Pt short termination to a coplanar waveguide to produce Rabi frequencies of ≈ 25 MHz. For the finite field measurements, magnetic fields were controlled to within 0.1 Gauss using three-axis Helmholtz coils. The temperatures quoted in the main text reflect measurements performed with an RTD adhered

*Present address: Institute for Molecular Engineering, University of Chicago, Chicago, Illinois 60637, USA

†Corresponding author. Email address: awsch@uchicago.edu

to the sample surface. The RTD and a lithographically patterned Ti/Pt resistive heater were connected to a PID feedback loop that stabilized the temperature, as measured by the RTD, to better than ±10 mK. Further details of the temperature control are provided in Ref. [1].

The sample was an electronic grade diamond from Element Six with natural ^{13}C abundance (1.1 %) that was irradiated with 2 MeV electrons (1 x 10^{14} cm^{-2}) and annealed in forming gas at 800 °C for 2 hours to increase the NV center density.

II. TEMPERATURE MEASUREMENT PROTOCOLS

First, let us consider temperature measurements in an external bias field B, between a few and a few hundred Gauss. In this regime, the NV center spin states (with $m_S = 0, -1,$ and $+1$, below referred to as $|0\rangle$, $|-1\rangle$, and $|+1\rangle$ respectively) are well-separated, and the NV center electron spin resonance (ESR) spectrum contains well-isolated lines corresponding to different ESR transitions, $|0\rangle \rightarrow |-1\rangle$ and $|0\rangle \rightarrow |+1\rangle$.

We compare the performance of three protocols: the regular Hahn echo on the $|0\rangle \rightarrow |-1\rangle$ transition, the thermal echo (TE), and the thermal CPMG (TCPMG). The general measurement scheme is the same for all of the protocols. We start with the NV center spin polarized in the state $|0\rangle$. We apply a preparation pulse $(\pi/2)_-$ at the frequency of the $|0\rangle \rightarrow |-1\rangle$ transition, which prepares a superposition $(1/\sqrt{2})[|0\rangle + |-1\rangle]$. The system then evolves under a given protocol. In the end, the phase between $|0\rangle$ and $|-1\rangle$ states is read out by applying another $(\pi/2)_-$ pulse, followed by the optical measurement of the probability for the NV center spin to be in the state $|0\rangle$.

A single period of the TE protocol has the structure

$$\tau - \pi_+\pi_-\pi_+ - \tau - \pi_-\pi_+\pi_-, \tag{1}$$

where π_- and π_+ are the π-pulses applied at the frequency of the $|0\rangle \rightarrow |-1\rangle$ and $|0\rangle \rightarrow |+1\rangle$ transitions, respectively, and τ denotes an inter-pulse delay. Note that the second triple of π-pulses is different from the first one. The TCPMG protocol is a symmetrized version of TE, and one period of TCPMG has the structure

$$\tau - \pi_+\pi_-\pi_+ - 2\tau - \pi_-\pi_+\pi_- - \tau, \tag{2}$$

so that the inter-pulse delays are placed symmetrically between the preparation and the readout pulses. The Hahn echo protocol is standard, $\tau - \pi_- - \tau$.

The Hamiltonian describing the NV center spin, placed in a magnetic field B (for simplicity in this discussion we ignore factors of $g\mu_{\rm B}$), subjected to a random quasi-static field δB, and interacting with the bath of ^{13}C nuclear spins has the form

$$H = DS_z^2 + (B + \delta B)S_z + S_z H_{B1} + H_{B2}. \tag{3}$$

S_z is the z-component operator of the NV center electronic spin (z-axis is directed along the [111] direction) and $D = 2\pi \cdot 2.87$ GHz is the NV center's zero-field splitting.

The third term includes the hyperfine coupling of the NV center spin to the bath of ^{13}C spins; since this coupling is much smaller than D, the value of S_z is a well-conserved quantity, so that the hyperfine coupling Hamiltonian does not include S_x and S_y. For the same reason, we neglected the contribution from the x- and y-components of the random field. The last term describes the internal dynamics of the ^{13}C nuclear spin bath. We assume that the NV center spin is subject to a magnetic field B which has a constant component and a random quasistatic component which causes dephasing. We aim to eliminate this quasistatic component and to minimize the influence of the ^{13}C spin bath.

Besides coupling with the ^{13}C spins, the NV center electronic spin is coupled to the intrinsic ^{14}N nuclear spin, and the corresponding hyperfine Hamiltonian has the form AS_zI_z (where I_z is the z-component of the ^{14}N nuclear spin). Since the ^{14}N spin remains static on the timescale of a single experimental run, this hyperfine coupling can be added to the δB field above, and as we will see below, is eliminated by the decoupling sequence.

First, let us consider the spin's evolution under the triples of π-pulses, and remember that the contribution from the bath of ^{13}C spins and from the random field δB can be neglected during short and strong pulses. For instance, let's take the second triple, $\pi_-\pi_+\pi_-$. It involves irradiation of the sample with microwave fields of two different frequencies, and it is more convenient to perform the analysis in the laboratory frame. We first apply a driving field at the frequency $\omega_1 = D - B$ of the $|0\rangle \rightarrow |-1\rangle$ transition; the action of the driving is described by the Hamiltonian term

$$H_{R1} = 2h_1 S_x \cos(\omega_1 t + \phi_1), \tag{4}$$

and the duration of the microwave pulse (t_{p1}) is adjusted to provide a π-rotation. The evolution can be analyzed in a frame rotating with frequency ω_1 using the standard secular approximation, and then re-cast back to the lab frame. In the rotating frame, defined by

the unitary transformation $\exp\left[it\omega_1 S_z\right] = \exp\left[it(D-B)S_z\right]$, we have the evolution operator

$$U_1' = \begin{pmatrix} \exp\left[-i(D+B+\omega_1)t_{p1}\right] & 0 & 0 \\ 0 & 0 & -i\exp\left(i\phi_1\right) \\ 0 & -i\exp\left(-i\phi_1\right) & 0 \end{pmatrix}. \tag{5}$$

The corresponding evolution operator in the lab frame is

$$U_1 = \begin{pmatrix} \exp\left[-i(D+B)t_{p1}\right] & 0 & 0 \\ 0 & 0 & -i\exp\left(i\phi_1\right) \\ 0 & -i\exp\left(-i\phi_1 - i\omega_1 t_{p1}\right) & 0 \end{pmatrix}. \tag{6}$$

Similarly, for the second π-pulse applied to the $|0\rangle \rightarrow |+1\rangle$ transition with frequency $\omega_2 = D + B$, with phase ϕ_2, and with the duration t_{p2}, the rotating frame is defined by the unitary transformation $\exp\left[-it\omega_2 S_z\right] = \exp\left[-it(D+B)S_z\right]$. The resulting evolution operator in the lab frame is

$$U_2 = \begin{pmatrix} 0 & -i\exp\left(-i\phi_2 - i\omega_2 t_{p2}\right) & 0 \\ -i\exp\left(i\phi_2\right) & 0 & 0 \\ 0 & 0 & \exp\left[-i(D-B)t_{p2}\right] \end{pmatrix}. \tag{7}$$

The full evolution operator in the lab frame under the triple of π-pulses is $U = U_+ U_- U_+$, and has a form:

$$U_{pmp} = -\begin{pmatrix} 0 & 0 & -\exp\left(-ia_1\right) \\ 0 & -\exp\left(-ia_2\right) & 0 \\ -\exp\left(-ia_3\right) & 0 & 0 \end{pmatrix}, \tag{8}$$

where the phase factors are $a_1 = \phi_2 - \phi_1 + 2Dt_{p2}$, $a_2 = (D+B)(t_{p2} + t_{p1})$, and $a_3 = \phi_1 - \phi_2 + (D-B)(t_{p1} + t_{p2})$. In a similar way, we can calculate the evolution operator for the other triple of π-pulses, to obtain

$$U_{mpm} = -\begin{pmatrix} 0 & 0 & -\exp\left(-iq_1\right) \\ 0 & -\exp\left(-iq_2\right) & 0 \\ -\exp\left(-iq_3\right) & 0 & 0 \end{pmatrix}, \tag{9}$$

with $q_1 = \phi_2 - \phi_1 + (D+B)(t_{p2} + t_{p1})$, $q_2 = (D-B)(t_{p1} + t_{p2})$, and $q_3 = \phi_1 - \phi_2 + 2Dt_{p1}$.

If the TE protocol (1) is applied to the initial state $|-1\rangle$, then the first inter-pulse delay produces the phase factor $\exp\left[-i\tau(D - B - \delta B)\right]$. Moreover, the coupling to the ^{13}C

spin bath produces a decoherence factor $V_{-1} = \exp[-i\tau(-H_{B1} + H_{B2})]$. Then, the first triple of pulses adds a phase a_3, and changes the state to $|+1\rangle$. The second inter-pulse delay produces the phase factor $\exp[-i\tau(D + B + \delta B)]$ and a decoherence factor $V_{+1} = \exp[-i\tau(H_{B1} + H_{B2})]$, which corresponds to $S_z = +1$. The final triple of pulses turns the state back to $|-1\rangle$, also adding the phase q_1. Thus, the initial state is transformed by the full protocol as follows:

$$|-1\rangle \to W_-|-1\rangle = \exp[-i(2\tau D + a_3 + q_1)]V_{+1}V_{-1}|-1\rangle. \tag{10}$$

If the initial state is $|0\rangle$, then each inter-pulse delay produces a decoherence factor $V_0 = \exp[-i\tau H_{B2}]$, and the total phase produced by the two π-pulse triples is $a_2 + q_2$. The total transformation is

$$|0\rangle \to W_0|0\rangle = \exp[-i(a_2 + q_2)]V_0^2|0\rangle. \tag{11}$$

A very useful feature of the protocol is the fact that the total phase a_2+q_2 added by pulses to the state $|0\rangle$ is the same as the total phase a_3+q_1 added by pulses to the state $|-1\rangle$ (also, the same is true for $|+1\rangle$). Thus, these phase factors do not affect the *mutual* phase between $|0\rangle$ and $|-1\rangle$, and can be omitted. In other words, the total signal remains independent of the duration of the pulses, independent of short delays between the π-pulses, and independent of the two microwave source phases. In fact, this property of the TE and TCPMG protocols holds for even more general patterns of the phase accumulation.

As a result, the measured signal S is determined only by the phase difference $2D\tau$ accumulated during the inter-pulse delays. The contributions from the external field, as well as from the random field and from the phases of the microwave sources, are cancelled. This ensures an excellent sensitivity of the method as is demonstrated in the main text. The signal $S(2\tau)$ oscillates rapidly with frequency D (close to 3 GHz) in the laboratory frame, and slowly decays on a timescale of tens to hundreds of microseconds due to decoherence from the ^{13}C spin bath.

This decay is the main factor limiting the accurate measurement of D. The envelope amplitude S_e of the measured signal is diminished due to entanglement with the ^{13}C spins, and is given by the expression

$$S_{e1} = \frac{1}{2} + \frac{1}{2}\mathrm{Re}\frac{\mathrm{Tr}_B[V_0^2(V_{+1}V_{-1})^\dagger]}{\mathrm{Tr}_B\mathbf{1}_B}. \tag{12}$$

The unitary operators of the bath $V_{0,\pm1}$ are given in Eqs. 10 and 11, and are just the conditional evolution operators of the bath corresponding to the NV center spin being in

the states $|0\rangle$ and $|\pm 1\rangle$, respectively. Tr_B denotes the trace over the bath, and $\mathbf{1}_B$ is the identity operator in the space of the bath, which ensures correct normalization.

A similar analysis can be performed for the TCMPG protocol. Again, it is easy to verify that the phase contributions from the pulses become irrelevant at the end of the protocol period, and the contributions from the external fields B and δB are cancelled as well. The signal $S(4\tau)$ also oscillates with frequency D in the laboratory frame. The impact of decoherence on the envelope S_e can also be calculated, and after a single TCPMG period it has the form

$$S_{e2} = \frac{1}{2} + \frac{1}{2}\mathrm{Re}\frac{\mathrm{Tr}_B[V_0^4(V_{-1}V_{+1}V_{+1}V_{-1})^\dagger]}{\mathrm{Tr}_B\mathbf{1}_B}, \tag{13}$$

where the decoherence term follows the sequence of the NV center spin states. For comparison, the decay of the spin echo envelope is given by

$$S_{e0} = \frac{1}{2} + \frac{1}{2}\mathrm{Re}\frac{\mathrm{Tr}_B[V_{-1}V_0(V_0V_{-1})^\dagger]}{\mathrm{Tr}_B\mathbf{1}_B}. \tag{14}$$

At very small magnetic fields, when the $|0\rangle \to |-1\rangle$ and $|0\rangle \to |+1\rangle$ transitions coalesce such that the $|-1\rangle$ and $|+1\rangle$ levels are almost degenerate, the temperature sensing protocols have simpler structures. A single π-pulse produces the simultaneous transformations (up to a common phase factor)

$$|-1\rangle \to |+1\rangle, \quad |0\rangle \to |0\rangle, \quad |+1\rangle \to |-1\rangle, \tag{15}$$

which at larger B requires the above-mentioned triples of π-pulses. Here, for clarity, we omitted the decoherence factors. The decoherence analysis can be performed in analogous manner to the case of the moderate-to-large B, and the conclusions are similar.

III. DECOHERENCE FROM THE NUCLEAR SPIN BATH

For an NV center spin decohered by a dilute nuclear spin bath, the fine quantitative details of the decoherence process are not universal [2–5]. They are determined by the specific positions of the nuclear spins around the given NV center, and change from one center to another. For instance, the initial shape of the signal decay (quadratic or quartic in time) is universal, but is limited to very short timescales. As we will see below, the long-time evolution is rather different from one NV center to another. Therefore, we aim to understand only the main qualitative features of the decoherence process.

At the relevant timescales, from ten to a hundred microseconds, the coupling between the ^{13}C nuclear spins can be neglected. The decoherence mechanism is the well-known effect of electron spin echo envelope modulation (ESEEM) [2, 6, 7]: each NV center spin state defines a different direction of the quantization axis for the nuclear spin ($\vec{m}_{0,\pm}$), and a different angular frequency for the nuclear spin precession ($\omega_{0,\pm}$). Therefore, the motion of each nuclear spin is conditioned on the electronic spin state, which leads to the entanglement with the ^{13}C spin bath and to the signal decay. In this case, the signal envelope S_e is a product of contributions of different spins, e.g. for TE protocol:

$$S_{e1} = \prod_k \left(\frac{1}{2} + \frac{1}{2} \mathrm{Re}\ \mathrm{Tr}_k [V_{0,k}^2 (V_{+1,k} V_{-1,k})^\dagger] \right). \tag{16}$$

Since the coupling between the ^{13}C nuclear spins is neglected, below we can consider the evolution of each nuclear spin separately, and omit the index k where it does not lead to confusion.

After appropriate rotation of the nuclear spin coordinate frame, the Hamiltonian of a ^{13}C spin can be written in the form

$$H_n = A S_z I_z + B S_z I_x + \omega_L I_z, \tag{17}$$

where I_z and I_x are the operators of the nuclear spin components, A and B are the hyperfine coupling constants, and ω_L is the nuclear spin Larmor frequency. As Eq. 12 shows, decoherence is determined by the overlap between two different evolutions of the ^{13}C spin: one, V_0, is the simple rotation under the action of only the external field. The other is the product of two rotations, first by the angle $\alpha_+ = \omega_+ \tau$ around the axis $\vec{m}_+$ (which corresponds to $S_z = +1$), and second by the angle $\alpha_- = \omega_- \tau$ around the axis $\vec{m}_-$ (corresponding to $S_z = -1$). The angular frequencies of the ^{13}C spin precessions are $\omega_\pm = \sqrt{(\omega_L \pm A)^2 + B^2}$. The resulting contribution to the TE signal is

$$\begin{aligned} S_{e1} \ &= \ \cos(\phi - \alpha_+ - \alpha_-) + (1 - m) \cos\phi \sin\alpha_+ \sin\alpha_- & (18) \\ &\quad -(1 - m_-^z) \sin\alpha_- \cos\alpha_+ \sin\phi - (1 - m_+^z) \sin\alpha_+ \cos\alpha_- \sin\phi, & (19) \end{aligned}$$

where $\phi = 2\omega_L \tau$ (total rotation angle during the period when the NV spin is in the state $|0\rangle$), the factors $m_\pm^z = (\omega_L \pm A)/\omega_\pm$ are the z-components of the conditional quantization axes $\vec{m}_\pm$, and the factor $m = \vec{m}_- \vec{m}_+ = (\omega_L^2 - B^2 - A^2)/(\omega_+ \omega_-)$. For comparison, the

contribution from the same ^{13}C spin to the Hahn echo signal is

$$S_{e0} = 1 - 2(m_-^x)^2 \sin^2(\phi/2) \sin^2(\alpha_-/2), \tag{20}$$

where $m_-^x = -b/\omega_-$ is the x-component of the conditional quantization axis $\vec{m}_-$.

For a typical NV center spin in medium external fields (10–100 G), the spread in the parameters A and B for different nuclear spins is large, and the angles $\alpha_\pm$ for different ^{13}C spins are effectively randomized between 0 and 2π on the timescale of the ^{13}C Larmor period ($t_L = 2\pi/\omega_L$). Thus, different terms in the expression for the TE signal (Eq. 18) have almost random phases, and the signal becomes completely decohered on the timescale t_L. At the same time, it is well known [2, 6, 7] that the Hahn echo signal becomes refocused at regular intervals, when $\phi/2$ becomes commensurate with π, and $S_{e0} = 1$ becomes independent of the randomized value of α_-. Note however, that the subsequent revivals of the Hahn echo are different from the initial decay. The initial decay corresponds to the short-time limit of Eq. 20, when $\sin(\alpha_-/2) \approx \alpha_-/2$, and has the approximate form $1 - t^4$. The subsequent revivals correspond to the randomized version of Eq. 20, when $\sin^2(\alpha_-/2) = 1/2$, and have the approximate form $1 - t^2$, i.e. they are narrower, but not as steep as the initial decay.

Therefore, the decay of the TE signal almost coincides with the initial decay of the Hahn echo only because the short-time limits of both expressions, Eq. 18 and 20, are the same (note that we do not assume smallness of A or B, only small τ):

$$S_e = 1 - \frac{1}{8} B^2 \omega_L^4 \tau^4. \tag{21}$$

This similarity, however, does not seem to have deeper physical meaning. The next terms in the short-time expansion are very different, $B^2\omega_L^2(A^2 + B^2 + 3\omega_L^2)\tau^6/144$ and $B^2\omega_L^2(A^2 + B^2 - 2A\omega_L + 2\omega_L^2)\tau^6/96$. The short-time expression for the symmetrized TCPMG protocol,

$$S_{e2} = 1 - \frac{1}{18} B^2 \omega_L^2 [B^2 + (A + 3\omega_L)^2)]\tau^6, \tag{22}$$

has a leading order of τ^6, reflecting the better performance expected for symmetrized protocols.

These considerations were checked with direct numerical simulations. 1200 ^{13}C spins were randomly placed on a diamond lattice with natural abundance, and the hyperfine coupling constants were calculated assuming only dipole-dipole interactions with the NV center spin. Renormalization of the ^{13}C g-factors [2] was neglected. Fig. 1 shows the simulated Hahn

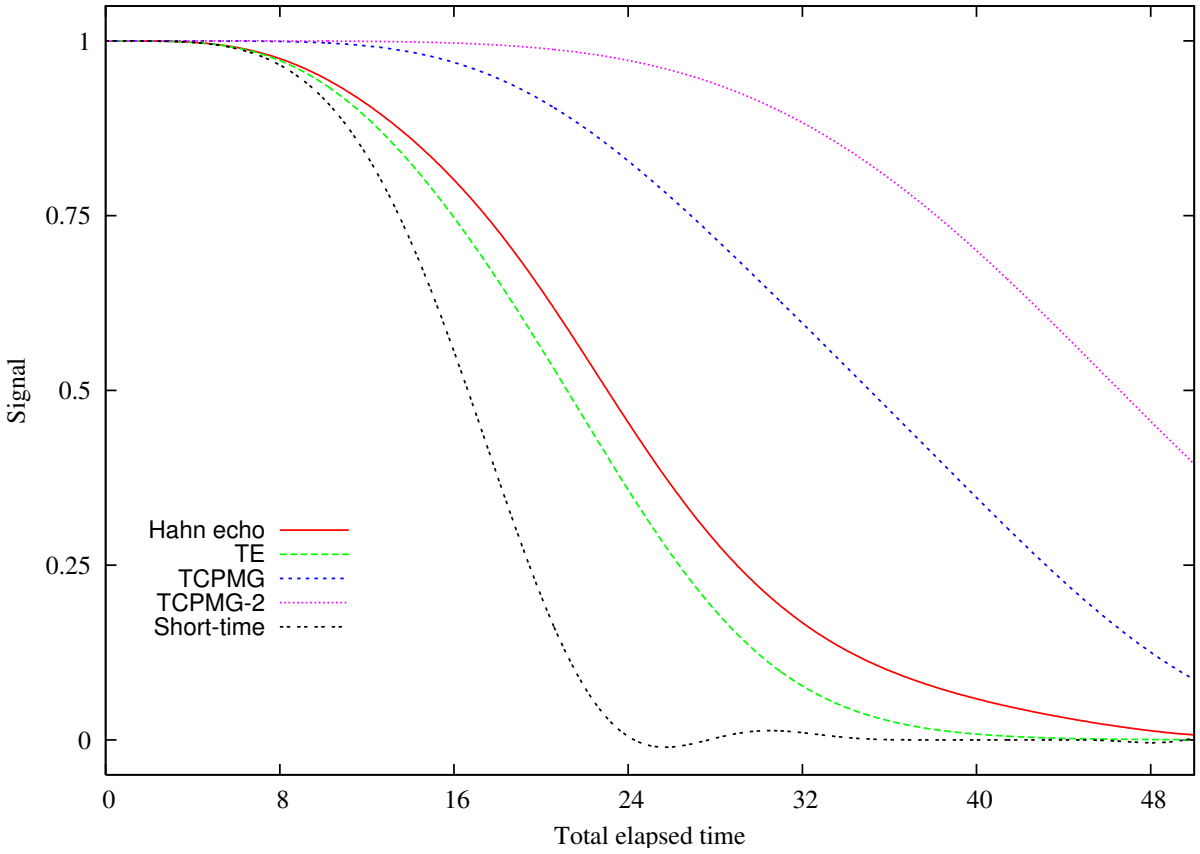

FIG. 1: Numerical modeling results for $B = 5$ G.

echo, TE, TCPMG, and TCPMG-2 signal envelopes, and compares them with the short-time approximation for the Hahn Echo and TE. Only small times are shown, since the short-time expression diverges for longer times. Also, at longer times the behavior of the temperature sensing protocols can noticeably vary for different NV centers with different geometrical arrangements of the surrounding ^{13}C nuclei.

IV. FURTHER CONSIDERATIONS FOR NV CENTER THERMOMETRY

A. Effects of strain, electric fields, and transverse magnetic fields

Our discussion in the main text does not explicitly include the effects of longitudinal or transverse strain on the TE and TCPMG-N sequences. In this work we consider the operation of NV center thermometers in magnetic fields large enough ($B_Z \geq 0.5$ G) such that transverse strain can be neglected ($|g\mu_B B_Z + A_{||} m_I| >> |\delta|$, where $A_{||}$ is the parallel

hyperfine coefficient, m_{I} is the spin projection of the nitrogen nuclear spin, and δ is the coupling of the $m_{\mathrm{S}} = +1$ and $m_{\mathrm{S}} = -1$ states induced by transverse strain). Longitudinal strains are more relevant, as they lead to variations in D among NV centers, and should be taken into account by calibrating D for each NV center if absolute thermometry is required. This strain variation is roughly 50 kHz [8], corresponding to a temperature uncertainty on the order of 1 K. For sensing relative temperature shifts, as we focus on here, these strains can be ignored. One alternative possibility for achieving absolute thermometry is through the use of NV center ensembles, such that the response of the ensemble corresponds to the mean value of D. However, in this case the variance of D would limit the achievable coherence times for the ensemble.

Longitudinal and transverse electric fields lead to analogous considerations as longitudinal and transverse strains [9]. Longitudinal electric fields produce relatively small shifts in D of 0.35 Hz cm V^{-1} [10]. These fields could become important in samples with a large density of optically ionizable impurities, as a fluctuating electric charge located ~ 20 nm from an NV center would produce shifts in D relevant for the ~ 85 μs coherence times observed in the main text. For high purity samples, as considered here, substitutional nitrogen impurities are assumed to be the most common charge traps and are specified to have a concentration less than 5 parts per billion. Similar to transverse strains, transverse electric fields can be neglected for the magnetic fields considered here.

Small magnetic fields transverse to the NV center's symmetry axis (B_{T}) also produce apparent shifts in D of magnitude $(g\mu_{\mathrm{B}}B_{\mathrm{T}})^2/(2D)$ that must be calibrated for absolute thermometry. For reasonable experimental conditions ($B_{\mathrm{T}} < 5$ G) these shifts are smaller than the quoted NV center to NV center variation in D. For sensing relative temperature shifts under such conditions the effects of B_{T} are negligible.

B. Microwave heating

Another relevant consideration for NV center thermometry is heating caused by absorption of the 2.87 GHz microwaves used for spin manipulation. Although this consideration is particularly relevant for liquid environments given the efficient absorption of microwaves by water, we note that three recent works probing NV center spins in cellular [11] or fluidic [12, 13] environments have provided no mention of heating caused by the CW microwaves

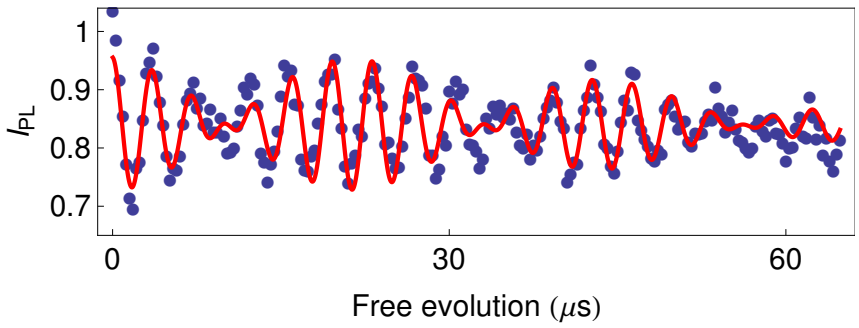

FIG. 2: TE measurement for an NV center with $B_Z \approx 0.5$ G. The microwave carrier frequency, Ω_{REF}, was detuned from D by ≈ 0.3 MHz to induce oscillations in I_{PL} to observe the signal envelope. The solid red line is a best fit to the data with Eq. 23.

utilized for ESR. Thermometry applications will also benefit from the long spin coherence times provided by the TE and TCPMG-N pulse sequences, as in these pulse sequences microwaves are applied for timescales of only ~ 100 ns out of 100 μs.

V. ADDITIONAL DATA

As mentioned in the main text, although we observe similar coherence enhancements with the TE and TCPMG-N pulse sequences on different NV centers, we have also observed modulations of the I_{PL} signal as a function of the free evolution time on other NV centers. This variance in response among NV centers is an important consideration for applications and also impacts the use of NV center ensembles for thermometry. Fig. 2 shows one example for a TE measurement performed on an NV center different from the one discussed in the main text with $B_Z \approx 0.5$ G. The solid red line is a best fit to the expression

$$I_{PL}(t) = a \exp\left(-\left(\frac{t}{\tau_{1/e}}\right)^3\right) \cos(\omega_1 t + \phi_1) \cos(\omega_2 t + \phi_2) + b, \tag{23}$$

where a, $\tau_{1/e}$, ω_1, ϕ_1, ω_2, ϕ_2, and b are free parameters. For this NV center the inhomogeneous spin lifetime (T_2^*) was 2.4 μs. The beating observed in this measurement appears qualitatively similar to features observed in the numerical modeling, suggesting it could be caused by a nearby ^{13}C, however, other possibilities such as the presence of a nearby photoionized impurity must also be considered.

[1] Toyli DM, *et al.* (2012) Measurement and control of single nitrogen-vacancy center spins above 600 K. *Phys Rev X* 2(3):031001.

[2] Childress L, *et al.* (2006) Coherent dynamics of coupled electron and nuclear spin qubits in diamond. *Science* 314(5797):281-285.

[3] Dobrovitski VV, Feiguin AE, Awschalom DD, & Hanson R (2008) Decoherence dynamics of a single spin versus spin ensemble. *Phys Rev B* 77(24):254212.

[4] Stanwix PL, *et al.* (2010) Coherence of nitrogen-vacancy electronic spin ensembles in diamond. *Phys Rev B* 82(20):201201.

[5] Witzel WM, Carroll MS, Cywinski L & Das Sarma S (2012) Quantum decoherence of the central spin in a sparse system of dipolar coupled spins. *Phys Rev B* 86(3):035452.

[6] Mims WB (1972) Envelope modulation in spin-echo experiments. *Phys Rev B* 5(7):2409-2419.

[7] Van Oort E & Glasbeek M (1990) Optically detected low field electron spin-echo envelope modulations of fluorescent N-V centers in diamond. *Chem Phys* 143(1):131-140.

[8] Hodges JS, *et al.* (2013) Timekeeping with electron spin states in diamond. *Phys Rev A* 87:032118.

[9] Dolde F, *et al.* (2011) Electric-field sensing using single diamond spins. *Nat Phys* 7(6):459-463.

[10] Van Oort E & Glasbeek M (1990) Electric-field-induced modulation of spin echoes of N-V centers in diamond. *Chem Phys Lett* 168(6):529-532.

[11] McGuiness LP, *et al.* (2011) Quantum measurement and orientation tracking of fluorescent nanodiamonds inside living cells. *Nat Nanotech* 6(6):358-363.

[12] Horowitz VR, Aleman BJ, Christle DJ, Cleland AN, & Awschalom DD (2012) Electron spin resonance of nitrogen-vacancy centers in optically trapped nanodiamonds. *Proc Natl Acad Sci U.S.A.* 109(34):13493-13497.

[13] Geiselmann M, *et al.* (2013) Three-dimensional optical manipulation of a single electron spin. *Nat Nanotech* 8(3):175-179.